Cancer Biol Med 2024. doi: 10.20892/j.issn.2095-3941.2023.0492

ORIGINAL ARTICLE

OPEN ACCESS

Calcification-associated molecular traits and therapeutic strategies in hormone receptor-positive HER2-negative breast cancer

Yuwei Li[1,2,3]*, Yuzheng Xu[1,2,3]*, Caijin Lin[1,2], Xi Jin[1,2], Ding Ma[1,2], Zhiming Shao[1,2,3]

[1]Department of Breast Surgery, Fudan University Shanghai Cancer Center, Shanghai 200032, China; [2]Key Laboratory of Breast Cancer in Shanghai, Fudan University Shanghai Cancer Center, Shanghai 200032, China; [3]Department of Oncology, Shanghai Medical College, Fudan University, Shanghai 200032, China

ABSTRACT

Objective: Mammographic calcifications are a common feature of breast cancer, but their molecular characteristics and treatment implications in hormone receptor-positive (HR+)/human epidermal growth factor receptor 2-negative (HER2−) breast cancer remain unclear.

Methods: We retrospectively collected mammography records of an HR+/HER2− breast cancer cohort (n = 316) with matched clinicopathological, genomic, transcriptomic, and metabolomic data. On the basis of mammographic images, we grouped tumors by calcification status into calcification-negative tumors, tumors with probably benign calcifications, tumors with calcification of low-moderate suspicion for maligancy and tumors with calcification of high suspicion for maligancy. We then explored the molecular characteristics associated with each calcification status across multiple dimensions.

Results: Among the different statuses, tumors with probably benign calcifications exhibited elevated hormone receptor immunohistochemical staining scores, estrogen receptor (ER) pathway activation, lipid metabolism, and sensitivity to endocrine therapy. Tumors with calcifications of high suspicion for malignancy had relatively larger tumor sizes, elevated lymph node metastasis incidence, Ki-67 staining scores, genomic instability, cell cycle pathway activation, and may benefit from cyclin-dependent kinase 4 and 6 (CDK4/6) inhibitors.

Conclusions: Our research established links between tumor calcifications and molecular features, thus proposing potential precision treatment strategies for HR+/HER2− breast cancer.

KEYWORDS HR+/HER2− breast cancer; mammographic calcifications; molecular features; precision treatment

Introduction

Breast cancer, the most common malignant tumor among women, poses a serious threat to women's health and lives[1]. Hormone receptor-positive (HR+)/human epidermal growth factor receptor 2-negative (HER2−) breast cancer, the most common subtype, accounts for approximately two-thirds of cases, and is characterized by the presence of the estrogen receptor (ER) and/or progesterone receptor (PR), and the absence of HER2 amplification[2]. Prior research has elucidated the molecular heterogeneity of HR+/HER2− breast cancer and proposed precision therapeutic strategies including endocrine therapy, cyclin-dependent kinase 4 and 6 (CDK4/6) inhibitors, and immunotherapy[3-8]. Nonetheless, the practical implementation of precision treatments on the basis of molecular features has several limitations. Further research is necessary to identify easily accessible clinical markers that link clinical presentation to molecular features and can predict various treatment outcomes.

Breast mammography, a routine clinical imaging examination, is crucial for early breast cancer screening and diagnosis[9-12]. Calcification is a common radiological feature in breast imaging and can be sensitively detected by mammography. Prior studies have reported elevated prevalence of

*These authors contributed equally to this work.
Correspondence to: Ding Ma and Zhiming Shao
E-mail: dma09@fudan.edu.cn and zhimin_shao@yeah.net
ORCID ID: https://orcid.org/0009-0000-4890-6424
and https://orcid.org/0000-0002-4503-148X
Received December 15, 2023; accepted February 19, 2024;
published online April 9, 2024.
Available at www.cancerbiomed.org

microcalcifications, a distinct type of calcification, in HR+ breast cancer, and have revealed that microcalcifications are associated with adverse clinicopathological characteristics and prognosis[13-17]. However, the underlying biological factors and their implications for clinical management require further exploration and clarification.

In this study, we established an integrative multi-omics cohort for HR+/HER2− breast cancer, incorporating mammographic images with clinicopathological, genomic, transcriptomic, and metabolomic data. This study was aimed at comprehensively investigating the biological characteristics associated with distinct mammographic calcification status, thereby aiding in the precision management and treatment of HR+/HER2− breast cancer.

Materials and methods

Patient samples and study cohorts

We established an HR+/HER2− breast cancer cohort with preoperative mammography (FUSCC-HR+/HER2− mammography). The samples were collected from patients with breast cancer who underwent surgery at Fudan University Shanghai Cancer Center (FUSCC) between January 2013 and December 2014. Detailed clinical information, pathological data, mammography reports, and follow-up data were recorded. Whole-exome sequencing, OncoScan, transcriptomic, and metabolomic data generation, as well as mammography image assessments, were as described in our prior research (IRB ID: 050432-4-1911D)[18,19]. Ethical approval for the use of all samples in this study was obtained from the FUSCC Ethics Committee.

Immunohistochemistry (IHC) analysis

Protein expression of specific genes in breast cancer tissues was detected with immunohistochemical staining on paraffin-embedded sections as follows. Deparaffinized slices were immersed in xylene, absolute ethanol, 95% ethanol, and 75% ethanol. The slices were then immersed in sodium citrate antigen retrieval solution and heated over water. Light-blocking was performed with peroxidase blocking solution for 30 min, and was followed by blocking with a 5% BSA solution for 1 h at room temperature. After TBST washing, the diluted antibodies (100 μL) were added dropwise, and the slices were incubated overnight at 4 °C. After TBST washing, corresponding secondary antibodies were added dropwise. DAB working solution was used for color development. Subsequently, the slides were sequentially immersed in 75% ethanol, 95% ethanol, absolute ethanol, and xylene. Finally, neutral resin was used for slide sealing. Immunohistochemistry scoring was determined by positive staining density, which was quantified with a computerized imaging system comprising a Leica charge-coupled device DFC420 camera connected to a Leica DM IRE2 microscope (Leica Microsystems Imaging Solutions). Densities were calculated by counting positive cells within an ×10 high-power field of view (~2 mm^2). Representative images of ER, PR, and Ki-67 are shown in **Figure S1**.

Prediction analysis of microarray 50-gene test classification

The determination of microarray 50-gene test (PAM50) subtypes was based on previously reported methods[20,21]. First, mRNA sequencing data were sampled to ensure that the proportion of IHC subtypes in the sample matched that of the training set used for PAM50 subtype determination. Subsequently, the FPKM data were adjusted according to the median expression values of PAM50 genes in the subset described above. Finally, PAM50 classification was determined according to the previously reported criteria.

Estimation of tumor mutational burden

Tumor mutational burden (TMB) was defined as the number of nonsynonymous somatic mutations per megabase (muts/Mb) within the coding region of the captured exome, encompassing missense, nonsense, nonstop, splice site, and translation start site mutations, as well as in-frame and frameshift insertions and deletions.

Estimation of the homologous recombination deficiency score and chromosomal instability score

The homologous recombination deficiency (HRD) score was the sum of the telomeric allelic imbalance (NtAI) score, loss of heterozygosity (LOH) score, and large-scale state transitions (LST) score. The telomeric allelic imbalance score indicated the count of subchromosomal regions exceeding 11 Mb with allelic imbalance extending to the telomere. The LOH score was determined by the number of LOH regions longer than 15 Mb but shorter than the entire chromosome (excluding

LOH regions on chromosome 17). The large-scale state transitions score was defined as the count of breakpoints between 2 chromosomal regions longer than 10 Mb after smoothing out regions shorter than 3 Mb. These scores were calculated with copy number data according to previous studies[22-26]. The chromosomal instability (CIN) score was derived by summing the squared gene-level GISTIC 2 values[27].

Gene set enrichment analysis and single-sample gene set enrichment analysis

Gene set enrichment analysis (GSEA) was conducted to investigate enriched pathways and interpret RNA-seq data, by using predefined gene sets from the Molecular Signatures Database (v.7.1) in GSEA software (v4.0). Default settings were applied for all basic and advanced fields.

Single-sample gene set enrichment analysis (ssGSEA) was used to calculate the characteristic pathway score with the "GSVA" function in the R package "GSVA"[28] (v1.42.0). Pathways were downloaded from the Bader laboratory.

Calculation of the sensitivity to endocrine therapy index and CDK4/6 inhibitor sensitivity score

The sensitivity to endocrine therapy index, used to indicate patients' sensitivity to endocrine therapy, was defined as follows: $\text{SET index} = \frac{G}{18} - \frac{R}{10} + 2$, where G is the sum of the expression of 18 informative genes (SLC39A6, STC2, CA12, ESR1, PDZK1, NPY1R, CD2, MAPT, QDPR, AZGP1, ABAT, ADCY1, CD3D, CD3D, MRPS30, DNAJC12, DNAJC12, SCUBE2, and KCNE4) and R is the sum of the expression of 10 reference genes (LDHA, ATP5J2, VDAC2, DARS, UGP2, UBE2Z, AK2, WIPF2, APPBP2, and TRIM2)[29-31]. Calculation of the CDK4/6 inhibitor sensitivity score was performed with the Gene Set Variation Analysis (GSVA) method with previously reported relevant genes (SAMD2, TIRAP, SETBP1, NNMT, TMSB10, KRT19, THBS2, MDK, EZH2, CDK4, CYR61, SORD, and GSTM3),[32] by using the "GSVA" function in the R package "GSVA"[28] (v1.42.0).

Metabolic pathway differential abundance score

Differential abundance (DA) scores reflect the tendency for pathways to have elevated levels of metabolites[33]. The DA score was calculated as (number of metabolites significantly increased or decreased)/number of measured metabolites within the pathway. DA scores range from −1 to 1. For a given pathway, scores of 1 indicated that all metabolites increased in abundance, whereas scores of −1 indicated that all metabolites decreased in abundance.

Correlation network of metabolites

First, the detected polar metabolites were included for further analysis[34]. Subsequently, a polar metabolite network was generated by calculation of Spearman's correlation, and negative correlations were not used. To achieve a concise representation and robust clustering effect, we retained metabolite interactions with correlation > 0.4 and FDR < 0.05, and removed the outlier nodes (KCore < 3) from the metabolite network. The ForceAtlas algorithm was used to lay out the structures for both networks[35], and correlation networks were visualized in Gephi (v0.9.3). Specific metabolites are also visualized in **Figure 5B**. Metabolites in distinct pathways were selected for visualization.

Statistical analysis

The Mann-Whitney Wilcoxon test and Kruskal–Wallis test were applied to analyze continuous variables, whereas Fisher's exact test was used to compare categorical variables. The *P* values for comparisons between pairs of groups among the 3 groups were calculated with the Mann-Whitney Wilcoxon test and adjusted for multiple comparisons with the Bonferroni method. Survival curves were constructed with the Kaplan–Meier product limit method and compared with the log-rank test. All analyses were performed in R (v4.1.1) (https://cran.r-project.org/).

Results

FUSCC-HR+/HER2− mammography cohort

To elucidate the molecular features associated with mammographic calcifications in HR+/HER2− breast cancer, we established a cohort of patients with HR+/HER2− breast cancer with preoperative mammography records (**Table 1**). Primary tumor samples were derived from patients treated at FUSCC between 2013 and 2014. Clinicopathological information and mammography images were collected in detail, in addition to whole exome sequencing (n = 271), OncoScan

Table 1 Clinicopathological characteristics of the cohort

	Calcification-negative	Probably benign	High suspicion	*P* value
	n (%)	*n* (%)	*n* (%)	
N	103	90	100	
Age, years (median)	55	58	52.5	
Breast density (%)				**0.011**
Entirely fatty	8 (7.8)	4 (4.4)	1 (1.0)	
Extremely dense	7 (6.8)	1 (1.1)	0 (0.0)	
Fibroglandular	54 (52.4)	54 (60.0)	66 (66.0)	
Heterogeneously dense	34 (33.0)	31 (34.4)	33 (33.0)	
Focal asymmetries (%)				0.290
Presence	15 (14.6)	21 (23.3)	18 (18.0)	
Absence	88 (85.4)	69 (76.7)	82 (82.0)	
Architectural distortion (%)				0.371
Presence	40 (38.8)	29 (32.2)	42 (42.0)	
Absence	63 (61.2)	61 (67.8)	58 (58.0)	
Lymph node status				**0.047**
Negative	51 (49.5)	50 (55.6)	38 (38.0)	
Positive	52 (50.5)	40 (44.4)	62 (62.0)	
Lympho-vascular invasion				**0.011**
Presence	46 (44.7)	30 (33.3)	58 (58.0)	
Absence	55 (53.4)	56 (62.2)	41 (41.0)	
Unknown	2 (1.9)	4 (4.4)	1 (1.0)	
Grade				0.183
Grade I	4 (3.9)	1 (1.1)	1 (1.0)	
Grade II	67 (65.0)	67 (74.4)	64 (64.0)	
Grade III	24 (23.3)	18 (20.0)	32 (32.0)	
Unknown	8 (7.8)	4 (4.4)	3 (3.0)	

P values were estimated on the basis of Fisher's exact test. *P* values less than 0.05 are displayed in bold.

($n = 199$), transcriptomics ($n = 312$), lipidomics ($n = 196$), and polar metabolomics ($n = 196$) data (**Figure 1**).

We assessed the mammography images according to the Breast Imaging Reporting and Data System (BI-RADS)[19,36,37] classification and categorized the calcification status accordingly (**Table S1**). Calcifications were divided into 3 groups with varying degrees of malignancy suspicion: calcifications assessed as BI-RADS 4C-5 were classified as having high suspicion for malignancy; calcifications assessed as BI-RADS 4A-4B were classified as having low-moderate suspicion for malignancy; and calcifications assessed as BI-RADS 2-3 were classified as probably benign. Tumors without calcifications were categorized as calcification-negative. Due to the limited sample size of patients with calcifications of low-moderate suspicion for malignancy ($n = 23$), subsequent analyses focused primarily on the remaining patients (**Figure 1**).

Thus, we established a multi-omics cohort of HR+/HER2− breast cancers with mammography images for further

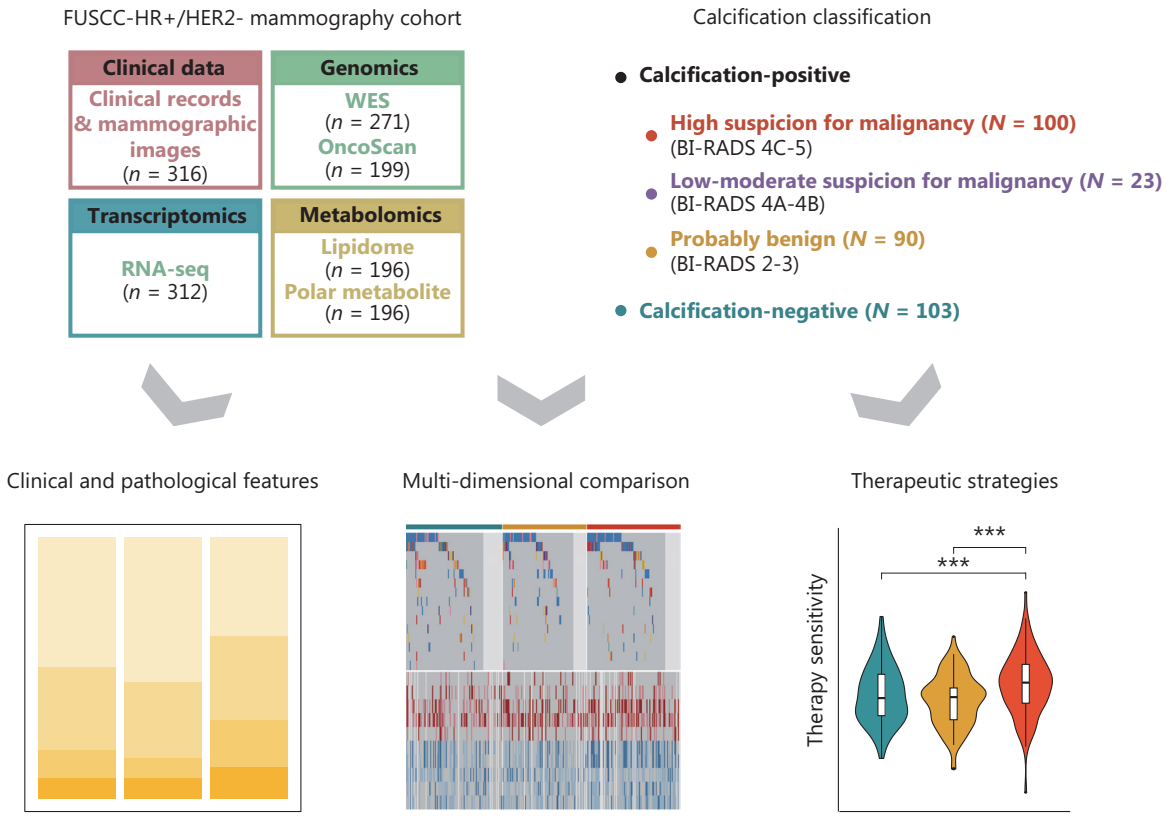

Figure 1 Schematic overview of the study design. A multi-omics cohort comprising 316 patients of breast cancer with mammography data. The cohort was stratified according to calcification features. Comparative analyses were conducted across clinicopathological characteristics, multi-omics dimensions, and precision therapeutic strategies.

exploration of biological features associated with calcifications, and related implications for precision treatment.

Clinical and pathological characteristics of tumors with different calcification statuses

We first focused on tumors with calcifications of high suspicion for malignancy. These tumors were associated with unfavorable clinicopathological characteristics, and were significantly larger than those in the other groups (in comparison to calcification-negative tumors, $P = 0.035$; in comparison to tumors with probably benign calcifications, $P = 0.061$, Mann-Whitney Wilcoxon test) (**Figure 2A**). These tumors also showed a higher rate of lymph node metastasis and lympho-vascular invasion than tumors without calcifications and tumors with probably benign calcifications (lymph node metastasis rate, 50.5% *vs.* 44.4% *vs.* 62.0%, $P < 0.001$, Fisher's exact test; lympho-vascular invasion rate, 45.5% *vs.* 34.9% *vs.* 58.6%, $P = 0.020$, Fisher's exact test) (**Figure 2B, C**). Moreover, this subset of tumors showed higher Ki-67 IHC staining scores than the other two groups (in comparison to calcification-negative tumors: $P = 0.184$; in comparison to tumors with probably benign calcifications, $P < 0.001$, Mann-Whitney Wilcoxon test) (median Ki-67 scores, 20% *vs.* 20% *vs.* 30%, $P = 0.001$, Kruskal-Wallis test) (**Figure 2E**). Furthermore, these tumors had higher histological grades than the other groups, although the difference did not reach statistical significance (**Figure S2**).

The patients with probably benign calcifications were significantly older than those with calcifications of high suspicion for malignancy ($P = 0.009$, Mann-Whitney Wilcoxon test) (**Figure 2D**), and their tumors exhibited higher ER and PR IHC staining scores than tumors with calcifications of high suspicion for malignancy ($P = 0.071$ and $P < 0.001$, respectively, Mann-Whitney Wilcoxon test) (**Figure 2E**).

Patients with probably benign calcifications tended to have better prognosis with endocrine therapy than the other patients, although this difference did not achieve

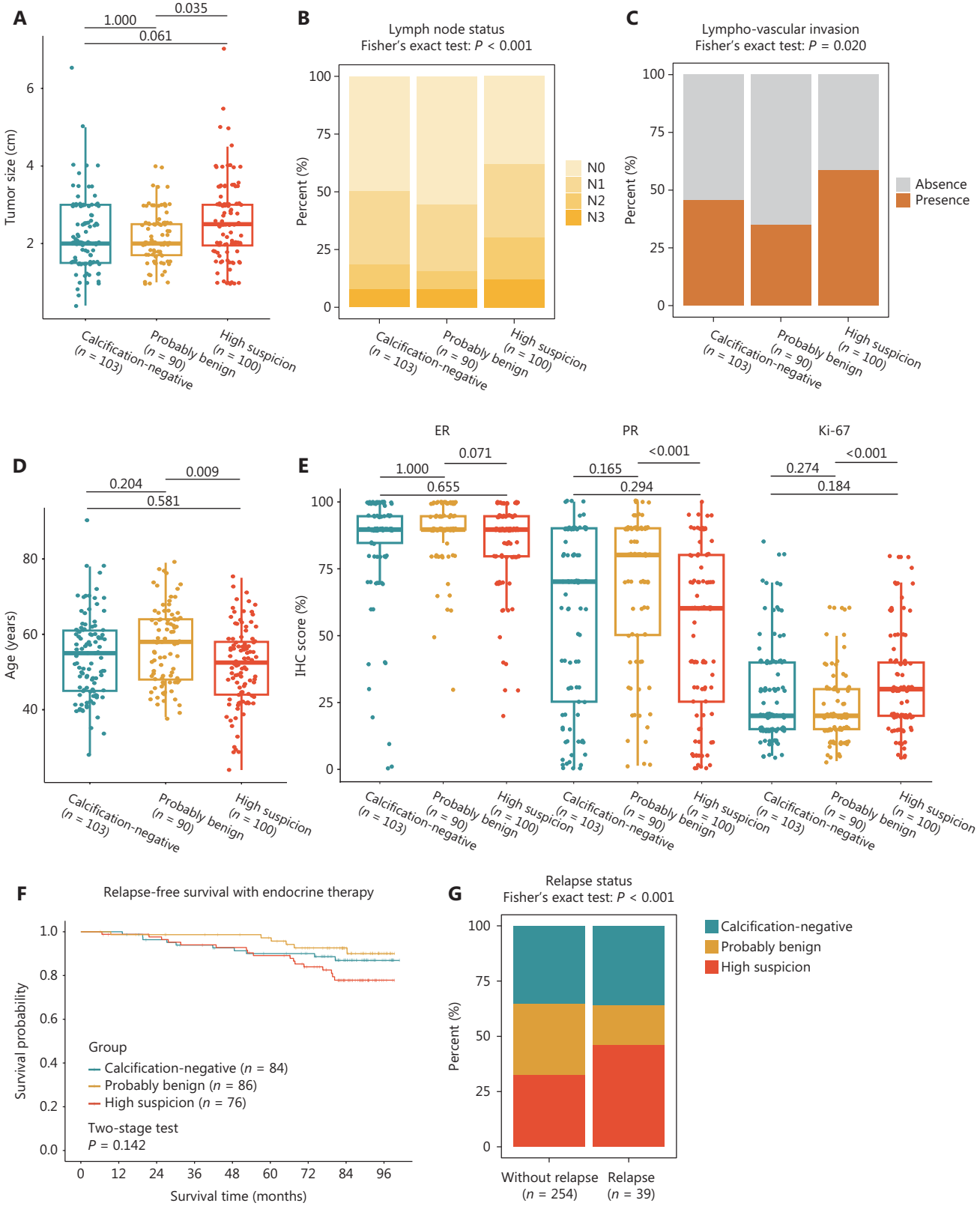

Figure 2 Clinical characteristics and pathological patterns of different calcification groups. (A) The box plot shows tumor sizes among groups. The sample sizes for the calcification-negative, probably benign, and high suspicion groups were 103, 90, and 100, respectively.

(B) The stacked bar chart compares the lymph node stages across groups. *P* values were calculated with Fisher's exact test. The sample sizes for the calcification-negative, probably benign, and high suspicion groups were 103, 90, and 100, respectively. (C) The stacked bar chart shows the lympho-vascular invasion status across groups. *P* values were calculated with Fisher's exact test. The sample sizes for the calcification-negative, probably benign, and high suspicion groups were 103, 90, and 100, respectively. (D) The box plot illustrates the ages among groups. The sample sizes for the calcification-negative, probably benign, and high suspicion groups were 103, 90, and 100, respectively. (E) The box plot shows the immunohistochemistry scores for ER, PR, and Ki-67. The sample sizes for the calcification-negative, probably benign, and high suspicion groups were 103, 90, and 100, respectively. (F) Relapse-free survival (RFS) among groups with endocrine therapy. *P* values were calculated from a two-stage test (probably benign *vs.* the others). (G) A stacked bar chart illustrates the calcification status for different recurrence outcomes. *P* values were calculated with Fisher's exact test.

statistical significance ($P = 0.142$, two-stage test) (**Figure 2F**). In addition, there was a higher rate of calcifications with high suspicion for malignancy in patients who relapsed compared to those who did not (46.2% *vs.* 33.5%, $P < 0.001$, Fisher's exact test) (**Figure 2G**).

Genomic features of tumors among calcification groups

To further understand the molecular features associated with mammographic calcification status, we compared the genomic features among groups. Overall, tumors with calcifications of high suspicion for malignancy had significantly higher tumor mutational burden (TMB), HRD scores, and CIN scores than the other groups (**Figure 3A-C**). We then analyzed mutational signatures specific to breast cancer and found no statistically significant differences (**Figure 3D**).

Mutational profiling indicated that the most frequently mutated cancer-associated genes in the cohort included *PIK3CA* (46%), *TP53* (26%), *GATA3* (14%), *MAP3K1* (15%), and *AKT1* (10%) (**Figure 3E**). We observed a higher mutation frequency of *MAP3K1* in the calcification-negative group than the other groups, but this difference did not reach statistical significance ($P = 0.080$, Fisher's exact test) (**Table S2**).

Furthermore, we systemically characterized somatic copy number variation (CNV) in the FUSCC-HR+/HER2− mammography cohort. Compared to tumors without calcification and those with probably benign calcifications, tumors with calcifications of high suspicion for malignancy displayed deletions in segments of chromosomes 17p (including *TP53*) and 11q (including *ATM*) (**Figure 3F**). Previous reports have suggested that the deletion of chromosome 17q is associated with cell cycle dysregulation[38]. Targeting the cell cycle is a crucial therapeutic approach in HR+/HER2− breast cancer[4-6,39,40]. Hence, we compared the copy number alteration frequency for each cell cycle-associated gene among the groups. Activation of the cell cycle was observed in tumors with calcifications of high suspicion for malignancy (**Figure 3G**). Notably, genes involved in positive regulation of the cell cycle exhibited an elevated amplification rate in these tumors. For example, the gain or amplification of *CCND2* was more pronounced than tumors with probably benign calcifications and those without calcifications (gain/amplification rate, 17.2% in calcification-negative groups *vs.* 8.4% in probably benign groups *vs.* 23.9% in high suspicion groups, $P = 0.023$, Fisher's exact test). Moreover, genes involved in the negative regulation of the cell cycle showed higher deletion rates in tumors with calcifications of high suspicion for malignancy; the loss or deletion frequency of *TP53* was highest among the 3 groups (loss/deletion rate: 39.8% *vs.* 45.8% *vs.* 71.6%, $P < 0.001$, Fisher's exact test).

In summary, we compared the genomic features of the different calcification groups and observed genomic instability and cell cycle activation in tumors with calcifications of high suspicion for malignancy.

Molecular characteristics and potential therapeutic strategies across distinct calcification groups, as inferred from transcriptomic data

To obtain deeper insights into the transcriptomic characteristics associated with calcifications, we first compared the compositions of established molecular subtypes among tumors differing in calcification status (**Figure 4A, B**). In the PAM50 subtyping system, the tumors with probably benign calcifications were composed primarily of luminal A and luminal B subtypes, in contrast to tumors without calcifications or with calcifications of high suspicion for malignancy (70.9% in calcification-negative groups *vs.* 91.0% in probably

benign groups *vs.* 81.6% in high suspicion groups, $P = 0.047$, Fisher's exact test) (**Figure 4A**). In regards to SNF subtype, a taxonomy of HR+/HER2- breast cancer we previously proposed based on this cohort[18], tumors with calcifications of high suspicion for malignancy were mainly SNF3 subtype, in contrast to tumors without calcifications and those with probably benign calcifications (27.1% *vs.* 29.4% *vs.* 49.2%, $P = 0.064$, Fisher's exact test) (**Figure 4B**). SNF3 tumors are characterized by activation of the cell cycle and HRD. The higher proportion of the SNF3 subtype was consistent with the higher Ki-67 staining scores (**Figure 2E**) and HRD scores (**Figure 3B**) observed in tumors with calcifications of high suspicion for malignancy.

Additionally, we curated treatment-associated signatures from the I-SPY2 study to assess molecular characteristics and potential treatment strategies in different groups, on the basis of the RNA data from our cohort (**Figure 4C**)[41]. Each group had unique features. Tumors without calcifications showed a highly immune-activated phenotype, tumors with probably benign calcifications showed a clear ER-associated signature,

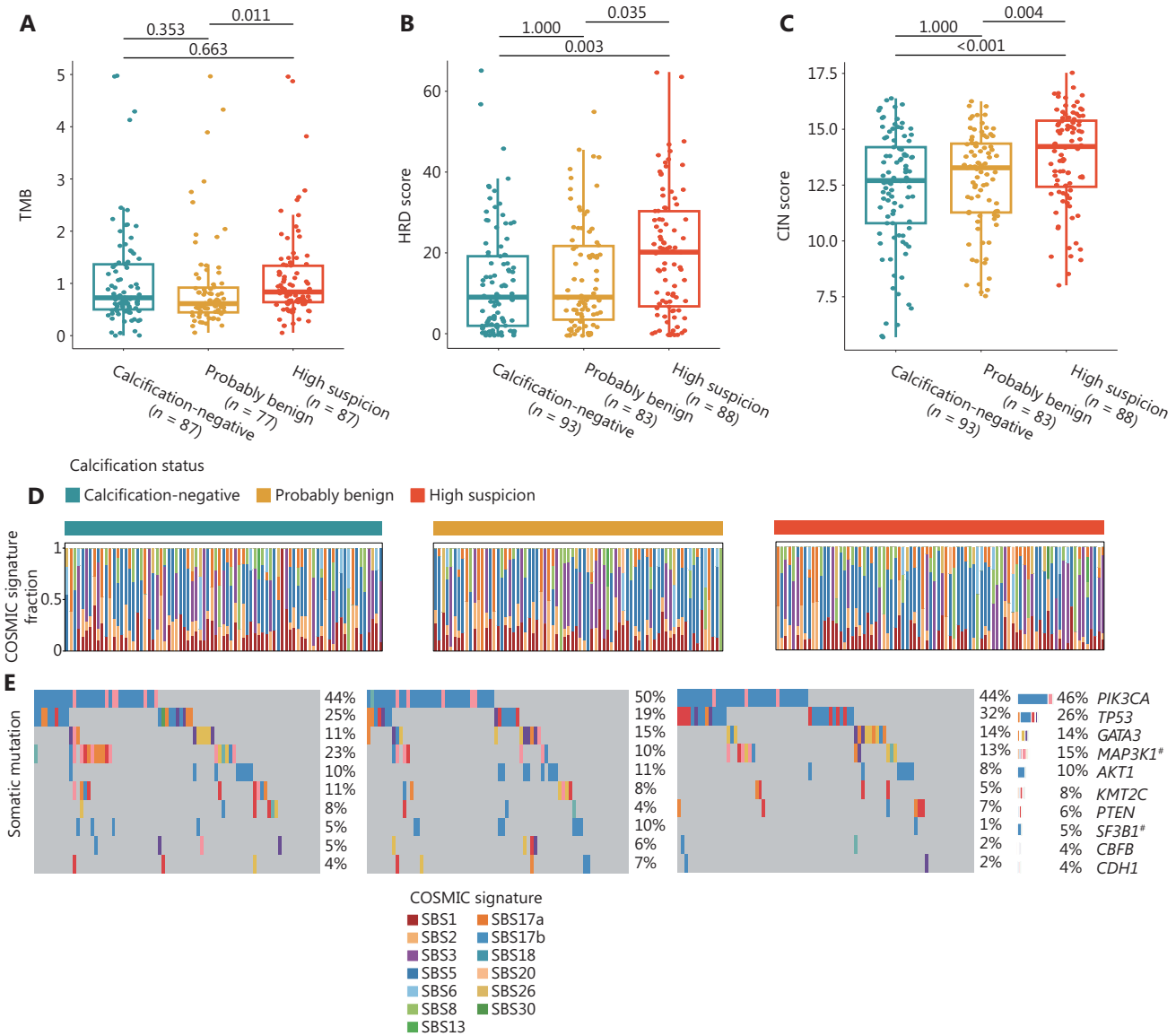

Figure 3 Continued

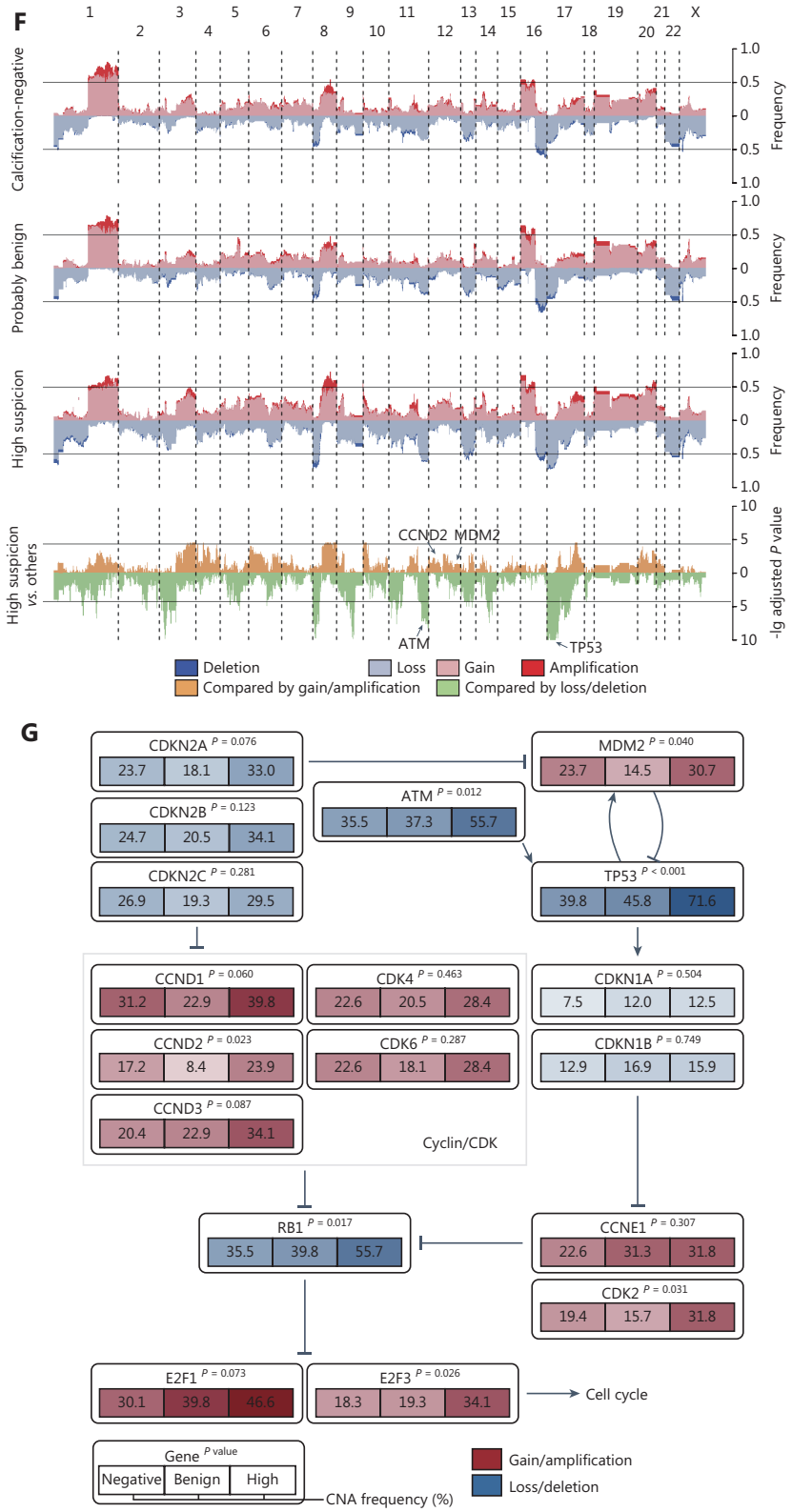

Figure 3 Genomic features of tumors in different calcification groups. (A) The box plot illustrates tumor mutational burden (TMB) scores among calcification groups. The sample sizes for the calcification-negative, probably benign, and high suspicion groups were 87, 77, and 87, respectively. (B) The box plot shows homologous recombination deficiency (HRD) scores across groups. The sample sizes for the

calcification-negative, probably benign, and high suspicion groups were 93, 83, and 88, respectively. (C) The box plot shows the comparison of chromosomal instability (CIN) scores. The sample sizes for the calcification-negative, probably benign, and high suspicion groups were 93, 83, and 88, respectively. (D) The proportion of mutation signatures in each sample, on the basis of the Catalog of Somatic Mutations in Cancer (COSMIC) database. (E) Somatic mutations of the top mutated genes. Genes are ordered by total mutation frequency. *P* values were calculated with Fisher's exact test (#*P* value < 0.1). (F) Somatic CNV among groups, and comparison between tumors with high suspicious calcifications and tumors in the other groups. The *P* values were calculated with Fisher's exact test and adjusted for multiple comparisons with the Bonferroni method; the horizontal line in the bottom panel represents the adjusted *P* value of 0.05. (G) The CNV frequencies of cell cycle genes across groups. *P* values were determined with Fisher's exact test.

and tumors with calcifications of high suspicion for malignancy displayed a high degree of proliferation.

Because the tumors among the three groups had distinct transcriptomic characteristics, we next explored the groups separately. Tumors without calcification exhibited immune activation; therefore, we used our RNA data to estimate the relative abundance of 24 microenvironmental cell types among the patients[42]. Tumors without calcification tended to have elevated infiltration of both adaptive and innate immune cells, thus suggesting a hot immune microenvironment (**Figure 4D**).

For tumors with probably benign calcifications, we performed ssGSEA and confirmed that the upregulation of ER-associated pathways in this subset of tumors, which originated from GSEA[43,44] (**Figure 4E**, **Table S3**). A previous study has indicated that ER pathway activation suggests sensitivity to endocrine therapy (ET)[45]. Therefore, we calculated the endocrine therapy index[29-31] for predicting sensitivity to ET. Tumors with probably benign calcifications were found to be more likely to benefit from ET (in comparison to calcification-negative tumors, $P = 0.019$; in comparison to high suspicion tumors, $P < 0.001$, Mann-Whitney Wilcoxon test) (**Figure 4F**).

Tumors with calcifications of high suspicion for malignancy showed higher ssGSEA scores for cell cycle-associated pathways (**Figure 4G**), thus indicating potential benefits of CDK4/6 inhibitor treatment. We calculated the sensitivity score for CDK4/6 inhibitors[32] and found that these tumors were predicted to have elevated sensitivity to CDK4/6 inhibitors (in comparison to calcification-negative tumors, $P = 0.007$; in comparison to probably benign tumors, $P < 0.001$, Mann-Whitney Wilcoxon test) (**Figure 4H**).

In summary, we further explored the molecular characteristics of tumors with various calcification statuses at the transcriptomic level and proposed treatment strategies that may enable calcification-assisted clinical management.

Metabolomic characteristics among calcification groups

Because metabolic reprogramming is a hallmark of cancer[46], we next explored the metabolic features associated with calcification. We performed metabolic pathway-based DA score analysis to describe the metabolic differences among calcification groups (**Figure 5A**)[47]. In tumors without calcification, we observed upregulation of vitamin metabolism (particularly thiamine metabolism) and downregulation of lipid metabolism. In tumors with probably benign calcification, thiamine metabolism was among the most down-regulated pathways. We also identified activation of lipid metabolism in these tumors, which has been associated with ER signaling in previous research[48]. In tumors with calcifications of high suspicion for malignancy, upregulation of amino acid metabolism (for example, tryptophan metabolism) was the most prominent metabolic feature. We subsequently conducted network analysis on specific polar metabolites, which indicated similar results (**Figure 5B**).

Discussion

To elucidate the molecular features associated with mammographic calcifications, we integrated a comprehensive multi-omics cohort of HR+/HER2− breast cancer with mammographic records. We classified the calcification status on the basis of mammographic images and conducted comprehensive investigations encompassing clinicopathological characteristics, genomics, transcriptomics, and metabolomics. In tumors without calcifications, the immune microenvironment was relatively hot. Tumors with probably benign calcifications displayed activation of the ER pathway, heightened responsiveness to endocrine therapy, and elevated lipid metabolism. Tumors with high suspicion calcifications exhibited larger tumor sizes; elevated prevalence of lymph node metastases, Ki-67 staining

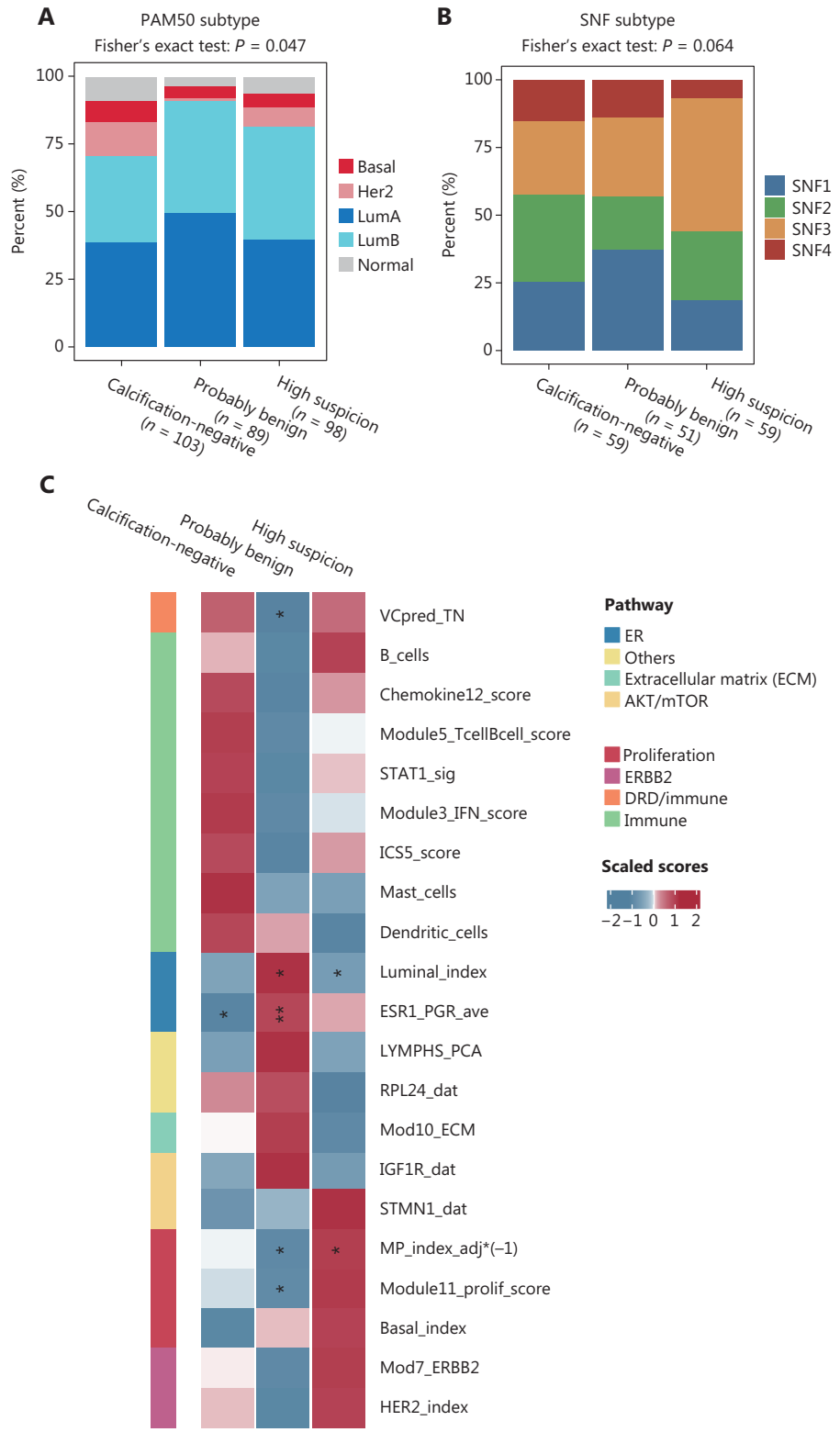

Figure 4 Continued

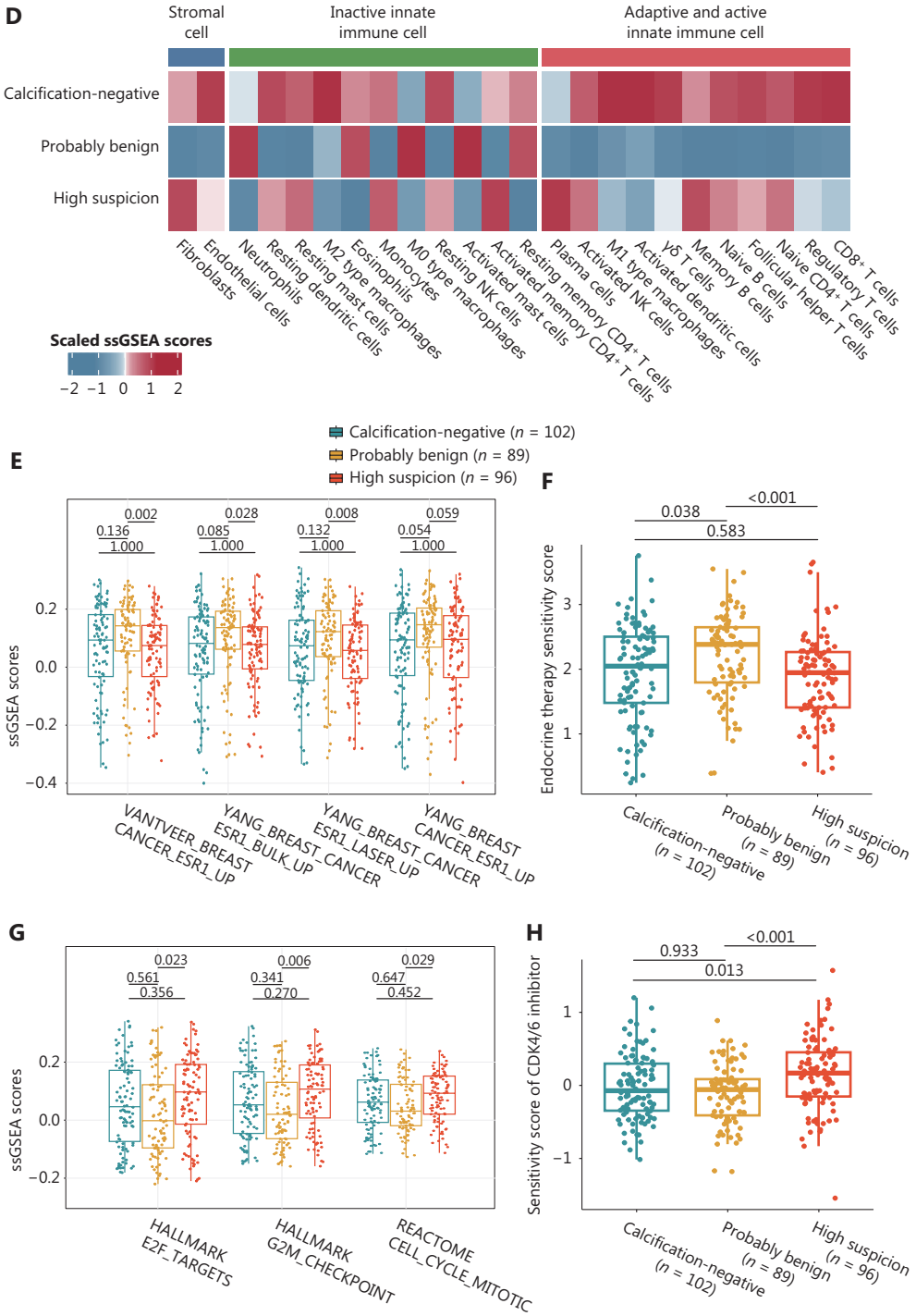

Figure 4 Exploration of transcriptomic features and therapeutic strategies among calcification groups. (A) The stacked bar chart shows the composition of PAM50 subtypes across groups. *P* values were calculated with Fisher's exact test. The sample sizes for the calcification-negative, probably benign, and high suspicion groups were 103, 89, and 98, respectively. (B) The stacked bar chart compares the composition of SNF subtypes across groups. *P* values were calculated with Fisher's exact test. The sample sizes for the calcification-negative, probably benign, and high suspicion groups were 59, 51, and 59, respectively. (C) The heatmap shows the comparison of biomarker scores. *P* values were determined with Mann-Whitney Wilcoxon tests (one group *vs.* the others) (*P value < 0.05; **P value < 0.01; ***P value < 0.001). (D) The heatmap reveals the estimated abundance of 24 microenvironment cell types. (E) The box plot shows the single-sample gene set enrichment analysis (ssGSEA) scores for ER-associated pathways. The sample sizes for the calcification-negative, probably benign, and high suspicion groups were 102, 89, and 96, respectively. (F) The box plots illustrate the sensitivity scores for endocrine therapy among groups. The sample sizes for the

calcification-negative, probably benign, and high suspicion groups were 102, 89, and 96, respectively. (G) The box plot shows the single-sample gene set enrichment analysis (ssGSEA) scores for cell cycle-associated pathways. The sample sizes for the calcification-negative, probably benign, and high suspicion groups were 102, 89, and 96, respectively. (H) The box plots compare the sensitivity scores for CDK4/6 inhibitors among groups. The sample sizes for the calcification-negative, probably benign, and high suspicion groups were 102, 89, and 96, respectively.

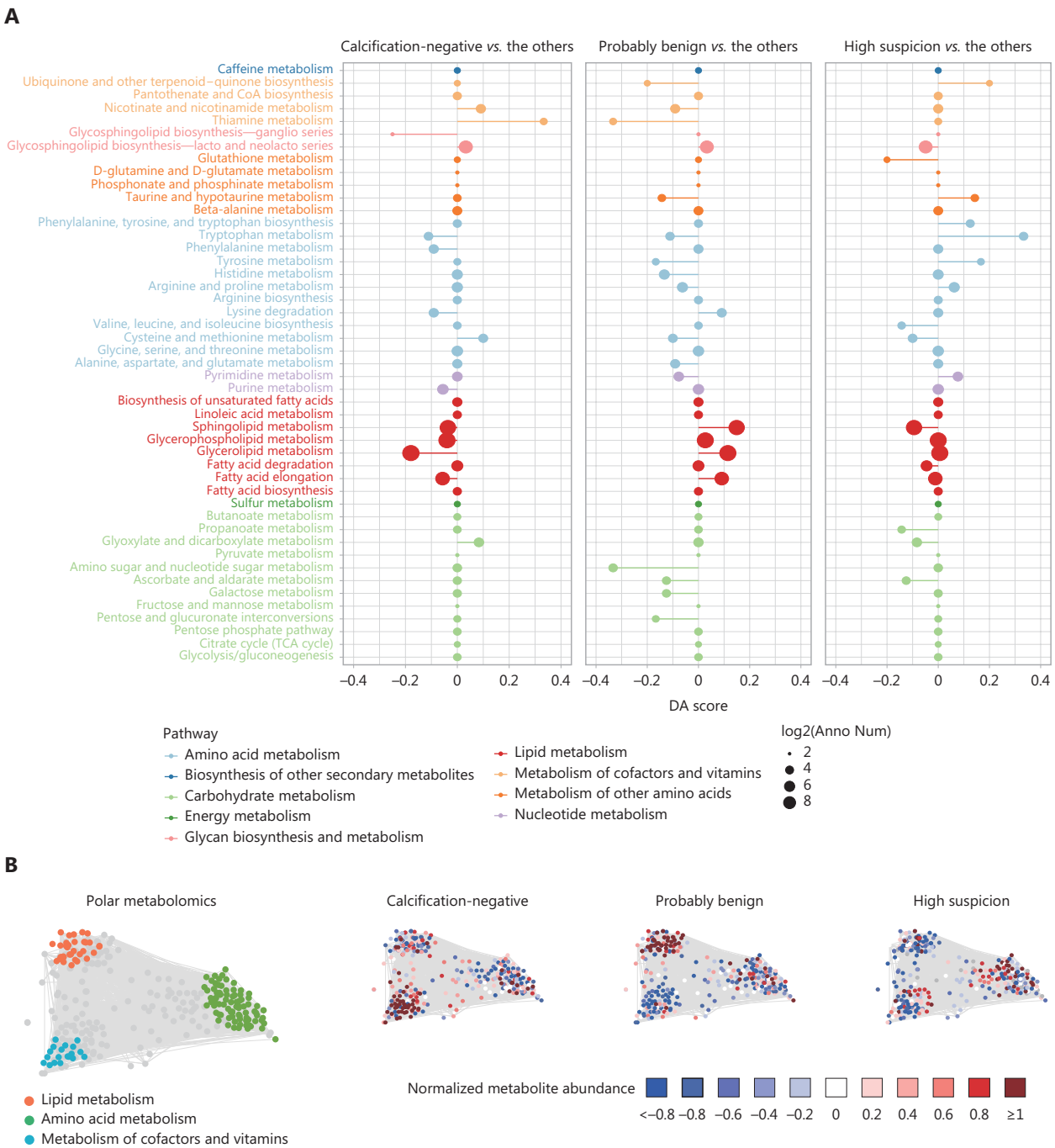

Figure 5 Exploratory analysis of metabolomic characteristics among calcification groups. (A) Pathway-based analysis of metabolomic changes among groups. The DA score captures the average gross changes for all metabolites in a pathway. A score of 1 indicates that all measured metabolites in the pathway increase, whereas a score of −1 indicates that all measured metabolites in a pathway decrease. (B) Differentially expressed metabolite correlation network based on polar metabolites with a >0.4 Spearman's correlation, FDR < 0.05. Correlation networks were partitioned by a graph-clustering algorithm, and the average quantification of groups in the correlation networks is presented.

scores, genomic instability, cell cycle pathway activation; and potential to respond positively to CDK4/6 inhibitors.

We previously investigated the molecular attributes of mammographic calcifications in triple-negative breast cancer[19]. However, similar studies had not been conducted in HR+/HER2− breast cancer. In our previous research, we conducted an in-depth exploration of the molecular heterogeneity within HR+/HER2− breast cancer, in a comprehensive multi-omics cohort[18]. This cohort enabled us to explore the molecular basis of tumors displaying various calcifications within HR+/HER2− breast cancer—a subtype constituting a substantial portion of breast cancer cases overall.

Our study demonstrated that the clinical and pathological characteristics of tumors with high suspicion calcifications were consistent with those previously observed in tumors with microcalcifications. We classified the calcifications on the basis of mammography images, by following established guidelines, and comprehensively considered the morphology and distribution factors of calcifications[37]. The presence of microcalcifications is correlated with larger tumor size, higher grade, positive axillary lymph node metastasis, and poorer prognosis in breast cancer[13,15,49,50]. We further identified molecular characteristics aligning with clinical features, including genomic instability and activation of the cell cycle pathway in tumors with high suspicion calcifications, thus potentially providing underlying explanations of malignant biological behaviors. Previous reports have suggested potential associations of the occurrence of these malignant calcifications with inflammation, calcium ions, and oxidative stress[14,51]. Our metabolomic analysis may offer a new perspective regarding the factors contributing to calcification formation.

Endocrine therapy is the standard treatment for HR+/HER2− breast cancer. However, previous studies have not reported a relationship between calcifications and this therapeutic approach. Therefore, an in-depth analysis of the biological characteristics underlying calcifications and their potential in guiding endocrine therapy was necessary. We observed that patients with probably benign calcifications tended to be older, to exhibit higher hormone receptor immunohistochemical scores, and to show ER-associated pathway activation than patients with other classifications. These findings collectively suggested that this subset of patients might favorably respond to endocrine therapy.

This study has several limitations. First, the sample size was limited, and the study cohort lacked randomization, thus necessitating the validation of key features and conclusions associated with the different calcification groups through external cohort data. Additionally, experimental validation will be essential for several of our observations and hypotheses, such as the sensitivity of tumors with high suspicion calcifications to CDK4/6 inhibitors.

Collectively, this study established a multi-omics cohort of HR+/HER2− breast cancer with mammography imaging, and further investigated the molecular characteristics and potential therapeutic strategies associated with various calcification states of tumors.

Grant support

This work was supported by grants from the National Key Research and Development Project of China (Grant No. 2020YFA0112304), the National Natural Science Foundation of China (Grant Nos. 81922048, 82072922, 91959207, and 92159301), the Program of Shanghai Academic/Technology Research Leader (Grant No. 20XD1421100), the Shanghai Key Laboratory of Breast Cancer (Grant No. 12DZ2260100), the Clinical Research Plan of SHDC (Grant Nos. SHDC2020CR4002 and SHDC2020CR5005), and the SHDC Municipal Project for Developing Emerging and Frontier Technology in Shanghai Hospitals (Grant No. SHDC12021103).

Conflict of interest statement

No potential conflicts of interest are disclosed.

Author contributions

Conceived and designed the analysis: Ding Ma, Zhiming Shao.
Collected the data: Yuwei Li, Yuzheng Xu.
Contributed data or analysis tools: Caijin Lin, Xi Jin.
Performed the analysis: Yuwei Li, Yuzheng Xu.
Wrote the paper: Yuwei Li, Yuzheng Xu.

Data availability statement

The data generated in this study are publicly available in the Genome Sequence Archive (GSA) database under accession code PRJCA017539 (https://ngdc.cncb.ac.cn/bioproject/browse/PRJCA017539).

References

1. Siegel RL, Miller KD, Jemal A. Cancer statistics, 2020. CA Cancer J Clin. 2020; 70: 7-30.
2. Huppert LA, Gumusay O, Idossa D, Rugo HS. Systemic therapy for hormone receptor-positive/human epidermal growth factor receptor 2-negative early stage and metastatic breast cancer. CA Cancer J Clin. 2023; 73: 480-515.
3. Pusztai L, Yau C, Wolf DM, Han HS, Du L, Wallace AM, et al. Durvalumab with olaparib and paclitaxel for high-risk HER22-negative stage II/III breast cancer: results from the adaptively randomized I- SPY2 trial. Cancer Cell. 2021; 39: 989-98.e5.
4. Sledge GW Jr., Toi M, Neven P, Sohn J, Inoue K, Pivot X, et al. The effect of abemaciclib plus fulvestrant on overall survival in hormone receptor-positive, ERBB2-negative breast cancer that progressed on endocrine therapy - MONARCH 2: a randomized clinical trial. JAMA Oncol. 2020; 6: 116-24.
5. Slamon DJ, Neven P, Chia S, Fasching PA, De Laurentiis M, Im SA, et al. Phase III randomized study of ribociclib and fulvestrant in hormone receptor-positive, human epidermal growth factor receptor 2-negative advanced breast cancer: MONALEESA-3. J Clin Oncol. 2018; 36: 2465-72.
6. Johnston SRD, Harbeck N, Hegg R, Toi M, Martin M, Shao ZM, et al. Abemaciclib combined with endocrine therapy for the adjuvant treatment of HR+, HER2−, node-positive, high-risk, early breast cancer (monarchE). J Clin Oncol. 2020; 38: 3987-98.
7. Manohar PM, Davidson NE. Updates in endocrine therapy for metastatic breast cancer. Cancer Biol Med. 2021; 19: 202-12.
8. Li J, Jiang Z. Chinese society of clinical oncology breast cancer (CSCO BC) guidelines in 2022: stratification and classification. Cancer Biol Med. 2022; 19: 769-73.
9. Smith RA, Andrews KS, Brooks D, Fedewa SA, Manassaram-Baptiste D, Saslow D, et al. Cancer screening in the united states, 2019: a review of current american cancer society guidelines and current issues in cancer screening. CA Cancer J Clin. 2019; 69: 184-210.
10. Conti A, Duggento A, Indovina I, Guerrisi M, Toschi N. Radiomics in breast cancer classification and prediction. Semin Cancer Biol. 2021; 72: 238-50.
11. Ding R, Xiao Y, Mo M, Zheng Y, Jiang YZ, Shao ZM. Breast cancer screening and early diagnosis in chinese women. Cancer Biol Med. 2022; 19: 450-67.
12. Huang Y, Wang H, Lyu Z, Dai H, Liu P, Zhu Y, et al. Development and evaluation of the screening performance of a low-cost high-risk screening strategy for breast cancer. Cancer Biol Med. 2021; 19: 1375-84.
13. Kim S, Tran TXM, Song H, Park B. Microcalcifications, mammographic breast density, and risk of breast cancer: a cohort study. Breast Cancer Res. 2022; 24: 96.
14. O'Grady S, Morgan MP. Microcalcifications in breast cancer: From pathophysiology to diagnosis and prognosis. Biochim Biophys Acta Rev Cancer. 2018; 1869: 310-20.
15. Tabar L, Chen HH, Duffy SW, Yen MF, Chiang CF, Dean PB, et al. A novel method for prediction of long-term outcome of women with T1a, T1b, and 10-14 mm invasive breast cancers: a prospective study. Lancet. 2000; 355: 429-33.
16. Azam S, Eriksson M, Sjolander A, Gabrielson M, Hellgren R, Czene K, et al. Mammographic microcalcifications and risk of breast cancer. Br J Cancer. 2021; 125: 759-65.
17. Qi X, Chen A, Zhang P, Zhang W, Cao X, Xiao C. Mammographic calcification can predict outcome in women with breast cancer treated with breast-conserving surgery. Oncol Lett. 2017; 14: 79-88.
18. Jin X, Zhou YF, Ma D, Zhao S, Lin CJ, Xiao Y, et al. Molecular classification of hormone receptor-positive HER2-negative breast cancer. Nat Genet. 2023; 55: 1696-708.
19. Lin CJ, Xiao WX, Fu T, Jin X, Shao ZM, Di GH. Calcifications in triple-negative breast cancer: molecular features and treatment strategies. NPJ Breast Cancer. 2023; 9: 26.
20. Parker JS, Mullins M, Cheang MC, Leung S, Voduc D, Vickery T, et al. Supervised risk predictor of breast cancer based on intrinsic subtypes. J Clin Oncol. 2009; 27: 1160-7.
21. Ciriello G, Gatza ML, Beck AH, Wilkerson MD, Rhie SK, Pastore A, et al. Comprehensive molecular portraits of invasive lobular breast cancer. Cell. 2015; 163: 506-19.
22. Timms KM, Abkevich V, Hughes E, Neff C, Reid J, Morris B, et al. Association of BRCA1/2 defects with genomic scores predictive of DNA damage repair deficiency among breast cancer subtypes. Breast Cancer Res. 2014; 16: 475.
23. Telli ML, Timms KM, Reid J, Hennessy B, Mills GB, Jensen KC, et al. Homologous recombination deficiency (HRD) score predicts response to platinum-containing neoadjuvant chemotherapy in patients with triple-negative breast cancer. Clin Cancer Res. 2016; 22: 3764-73.
24. Abkevich V, Timms KM, Hennessy BT, Potter J, Carey MS, Meyer LA, et al. Patterns of genomic loss of heterozygosity predict homologous recombination repair defects in epithelial ovarian cancer. Br J Cancer. 2012; 107: 1776-82.
25. Birkbak NJ, Wang ZC, Kim JY, Eklund AC, Li Q, Tian R, et al. Telomeric allelic imbalance indicates defective DNA repair and sensitivity to DNA-damaging agents. Cancer Discov. 2012; 2: 366-75.
26. Popova T, Manie E, Rieunier G, Caux-Moncoutier V, Tirapo C, Dubois T, et al. Ploidy and large-scale genomic instability consistently identify basal-like breast carcinomas with BRCA1/2 inactivation. Cancer Res. 2012; 72: 5454-62.
27. Ock CY, Hwang JE, Keam B, Kim SB, Shim JJ, Jang HJ, et al. Genomic landscape associated with potential response to anti-CTLA-4 treatment in cancers. Nat Commun. 2017; 8: 1050.
28. Hanzelmann S, Castelo R, Guinney J. GSVA: Gene set variation analysis for microarray and RNA-seq data. BMC Bioinformatics. 2013; 14: 7.
29. Du L, Yau C, Brown-Swigart L, Gould R, Krings G, Hirst GL, et al. Predicted sensitivity to endocrine therapy for stage II-III hormone receptor-positive and HER2-negative (HR+/HER2−) breast cancer before chemo-endocrine therapy. Ann Oncol. 2021; 32: 642-51.

30. Speers CW, Symmans WF, Barlow WE, Trevarton A, The S, Du L, et al. Evaluation of the sensitivity to endocrine therapy index and 21-gene breast recurrence score in the SWOG S8814 trial. J Clin Oncol. 2023; 41: 1841-8.
31. Sinn BV, Fu C, Lau R, Litton J, Tsai TH, Murthy R, et al. Set(ER/PR): a robust 18-gene predictor for sensitivity to endocrine therapy for metastatic breast cancer. NPJ Breast Cancer. 2019; 5: 16.
32. Finn RS, Liu Y, Zhu Z, Martin M, Rugo HS, Dieras V, et al. Biomarker analyses of response to cyclin-dependent kinase 4/6 inhibition and endocrine therapy in women with treatment-naive metastatic breast cancer. Clin Cancer Res. 2020; 26: 110-21.
33. Xiao Y, Ma D, Yang YS, Yang F, Ding JH, Gong Y, et al. Comprehensive metabolomics expands precision medicine for triple-negative breast cancer. Cell Res. 2022; 32: 477-90.
34. Chen D, Zhang Y, Wang W, Chen H, Ling T, Yang R, et al. Identification and characterization of robust hepatocellular carcinoma prognostic subtypes based on an integrative metabolite-protein interaction network. Adv Sci (Weinh). 2021; 8: e2100311.
35. Chen YJ, Roumeliotis TI, Chang YH, Chen CT, Han CL, Lin MH, et al. Proteogenomics of non-smoking lung cancer in East Asia delineates molecular signatures of pathogenesis and progression. Cell. 2020; 182: 226-44.e17.
36. American College of Radiology; D'Orsi CJ, Sickles EA, Mendelson EB, Morris EA. ACR BI-RADS atlas: breast imaging reporting and data system; mammography, ultrasound, magnetic resonance imaging, follow-up and outcome monitoring, data dictionary. American College of Radiology; 2013.
37. Spak DA, Plaxco JS, Santiago L, Dryden MJ, Dogan BE. BI-RADS® fifth edition: a summary of changes. Diagn Interv Imaging. 2017; 98: 179-90.
38. Edelmann J, Holzmann K, Tausch E, Saunderson EA, Jebaraj BMC, Steinbrecher D, et al. Genomic alterations in high-risk chronic lymphocytic leukemia frequently affect cell cycle key regulators and NOTCH1-regulated transcription. Haematologica. 2020; 105: 1379-90.
39. Thu KL, Soria-Bretones I, Mak TW, Cescon DW. Targeting the cell cycle in breast cancer: towards the next phase. Cell Cycle. 2018; 17: 1871-85.
40. Bai J, Li Y, Zhang G. Cell cycle regulation and anticancer drug discovery. Cancer Biol Med. 2017; 14: 348-62.
41. Wolf DM, Yau C, Wulfkuhle J, Brown-Swigart L, Gallagher IR, Lee PRE, et al. Redefining breast cancer subtypes to guide treatment prioritization and maximize response: predictive biomarkers across 10 cancer therapies. Cancer Cell. 2022; 40: 609-23.e6.
42. Xiao Y, Ma D, Zhao S, Suo C, Shi J, Xue MZ, et al. Multi-omics profiling reveals distinct microenvironment characterization and suggests immune escape mechanisms of triple-negative breast cancer. Clin Cancer Res. 2019; 25: 5002-14.
43. van' t Veer LJ, Dai H, van de Vijver MJ, He YD, Hart AA, Mao M, et al. Gene expression profiling predicts clinical outcome of breast cancer. Nature. 2002; 415: 530-6.
44. Yang F, Foekens JA, Yu J, Sieuwerts AM, Timmermans M, Klijn JG, et al. Laser microdissection and microarray analysis of breast tumors reveal ER-alpha related genes and pathways. Oncogene. 2006; 25: 1413-9.
45. Symmans WF, Hatzis C, Sotiriou C, Andre F, Peintinger F, Regitnig P, et al. Genomic index of sensitivity to endocrine therapy for breast cancer. J Clin Oncol. 2010; 28: 4111-9.
46. Hanahan D. Hallmarks of cancer: new dimensions. Cancer Discov. 2022; 12: 31-46.
47. Hakimi AA, Reznik E, Lee CH, Creighton CJ, Brannon AR, Luna A, et al. An integrated metabolic atlas of clear cell renal cell carcinoma. Cancer Cell. 2016; 29: 104-16.
48. Kulkoyluoglu-Cotul E, Arca A, Madak-Erdogan Z. Crosstalk between estrogen signaling and breast cancer metabolism. Trends Endocrinol Metab. 2019; 30: 25-38.
49. Zheng K, Tan JX, Li F, Wei YX, Yin XD, Su XL, et al. Relationship between mammographic calcifications and the clinicopathologic characteristics of breast cancer in western china: a retrospective multi-center study of 7317 female patients. Breast Cancer Res Treat. 2017; 166: 569-82.
50. Kwon BR, Shin SU, Kim SY, Choi Y, Cho N, Kim SM, et al. Microcalcifications and peritumoral edema predict survival outcome in luminal breast cancer treated with neoadjuvant chemotherapy. Radiology. 2022; 304: 310-9.
51. Cox RF, Hernandez-Santana A, Ramdass S, McMahon G, Harmey JH, Morgan MP. Microcalcifications in breast cancer: novel insights into the molecular mechanism and functional consequence of mammary mineralisation. Br J Cancer. 2012; 106: 525-37.

Cite this article as: Li Y, Xu Y, Lin C, Jin X, Ma D, Shao Z. Calcification-associated molecular traits and therapeutic strategies in hormone receptor-positive HER2-negative breast cancer. Cancer Biol Med. 2024; x: xx-xx. doi: 10.20892/j.issn.2095-3941.2023.0492